Differentially rotating split-cylinder flow: Responses to weak harmonic forcing in the rapid rotation regime

Paloma Gutierrez-Castillo* and Juan M. Lopez†
School of Mathematical and Statistical Sciences, Arizona State University, Tempe, Arizona 85287, USA
(Received 7 April 2017; published 24 August 2017)

The flow in a rapidly rotating cylinder is studied numerically. The cylinder is split in half, and the rapid rotation in the two halves is modulated harmonically with a small amplitude. We consider modulation frequencies ranging from zero to twice the background rotation frequency, so that the system supports inertial waves. The split in the cylinder at midheight provides a localized perturbation from which inertial wave beams emanate, but so too do the corners where the endwalls and the sidewall meet. There is no discontinuity in the boundary condition at these corners, but the thin modulated endwall and sidewall boundary layers meet at the corners, and this leads to a localized perturbation to the rapid background rotation. This interaction produces inertial wave beams that over wide parameter regimes are more intense than those from the split at the cylinder midheight. Due to finite viscosity and nonlinear flow conditions, the wave beams produce intricate patterns formed by constructive and destructive interference as they self-intersect and reflect off cylinder boundaries and the axis. These patterns are very sensitive to the modulation frequency. Additionally, a phase difference between the modulations of the two cylinder halves was imposed. The phase difference impacts the symmetries of the system and its response to the modulations. In particular, some low-order Kelvin modes are driven resonantly, and their selection depends not only on the frequency but also on the phase of the differential modulation.

DOI: 10.1103/PhysRevFluids.2.084802

I. INTRODUCTION

Rapidly rotating confined flow subjected to small-amplitude periodic forcing can have large-amplitude responses. This has been linked to catastrophic failures in spin-stabilized spacecrafts [1,2], as well as dynamo action and various instabilities in liquid-core planets [3–6]. The study of small perturbations to rapidly rotating flows has a long history, going back at least to Lord Kelvin [7], who idealized the problem by neglecting the viscous terms, and linearized about the state of solid-body rotation. In the cylinder, he used separation of variables to solve the resulting eigenvalue problem, and these eigenmodes are now called Kelvin modes. Much fundamental insight has been gleaned by studying the linear inviscid limit; see the texts by Greenspan [8], and more recently by Davidson [9], for overviews. The linear inviscid problem is hyperbolic and supports waves known as inertial waves. These have peculiar properties, such as the group velocity at which energy propagates away from a disturbance in the form of wave-packets being perpendicular to the phase velocity. Thus, a wave-packet propagates at right angles to the apparent direction of propagation of the wave crest. The inertial waves travel in the direction of the characteristics; the so-called rays travel on cones of angle $\beta = \arccos(\omega_p/2\Omega)$ with respect to a plane normal to the rotation axis, where ω_p is the perturbation frequency and Ω is the solid-body rotation frequency.

Often [10–14] the question is raised whether a periodically forced confined rapidly rotating system resonantly excites Kelvin modes. The cylinder is one of a handful of geometries which are separable, yet even for the cylinder the completeness of the cylinder Kelvin modes remains an open question

*paloma.gutierrez.1@asu.edu
†jmlopez@asu.edu

[15]. For finite viscosity, the eigenmodes corresponding to infinitesimal perturbations of confined solid-body rotation are the eigenmodes of the Navier-Stokes equations linearized about solid-body rotation. These "viscous modes" are often very similar to Kelvin modes. In geometries such as the cylinder, the viscous modes and the Kelvin modes differ primarily in the boundary layer structures that are present in the viscous modes that accommodate the no-slip boundary condition [16–18]. What happens when there is periodic forcing? From the perspective of an initial-value problem, if the Kelvin modes were complete the initial condition could be described as a combination of these. For the viscous problem, the viscous modes can be combined to describe the initial condition; these are viscously damped, and one is left with the forced response (often referred to as the "steady-state"). How is the forced response related to the imposed forcing and to the eigenmodes (viscous or inviscid) of the container? Further complicating the issue is the fact that for finite viscosity there are also internal shear layers that, for example, in periodically forced cylinder flows, emerge from the corners where endwalls and the sidewall meet. Wood [19,20] first suggested their occurrence analytically, and they have been subsequently observed experimentally [21] and numerically [22,23], and in combined experimental and numerical studies [24]. When the forcing is axisymmetric, these internal shear layers are conical with cone angle in accord with the dispersion relation derived from the linear inviscid theory. When the forcing or the geometry are not axisymmetric, the shear layers do not form axisymmetric cones (e.g., see Refs. [18] for precessional forcing of a cylinder and [25] for librational forcing of a cube). These internal shear layers have been associated with the characteristics of the corresponding linear inviscid idealized flow, and interpreted as being viscous regularizations of singular surfaces [19,20]. Baines [26] raises some concerns about such an interpretation; the analysis of Wood involves the singular perturbation of neglecting viscous effects, leading to an ill-posed hyperbolic boundary value problem (BVP). The idealization of ignoring viscous and nonlinear terms in the governing equations is ostensibly made for the purpose of making the problem analytically tractable, and this comes at the expense of not being able to account for the physical no-slip boundary conditions, introducing ill-posedness and subsequent pathologies that may not have physical significance. Greenspan [27] discusses this, noting that the spectrum being dense results from the failure of the asymptotic method to locate the eigenvalues properly. This stems from the fact that the viscous problem in the limit of small viscosity has boundary layers, and when the wavelength of the inviscid eigenmodes is comparable to the boundary layer thickness, the concept of an inviscid interior flow with a viscous boundary layer correction breaks down. McEwan [21] also notes that "there arise from the linearized inviscid solutions for cylindrically bounded motions features of questionable physical validity." A problem with the hyperbolic BVP is that infinitesimal changes in the system parameters change the distribution of characteristic surfaces within the container from retracing to nonretracing. For real (viscous) fluids, these difficulties might be regarded as artificial since the system is then elliptic and well-posed. Nevertheless, some aspects of the results from the hyperbolic BVP are found to be useful (the dispersion relation and eigenmodes), but it remains unclear to what extent the response to external forcing can be predicted without consideration of the Navier-Stokes equations with no-slip boundary conditions.

A further issue that has been recently raised is how is the symmetry of the response related to the symmetry of the forcing? Often it is claimed that the response can only consist of Kelvin modes whose frequencies are sufficiently close to the forcing frequency and whose spatial structure has the same symmetry as the forcing [24,25,28]. These observations are made based on considerations of forcing with symmetry. A corollary question is what is the response when the forcing does not have symmetry?

The Kelvin modes of the cylinder have azimuthal symmetries, characterized by m, the azimuthal wave number. If the forcing is axisymmetric and sufficiently small so that the response is also small, then the response will also be axisymmetric. With librational forcing, symmetry breaking in the sidewall boundary layer is found both experimentally and numerically when the Rossby number (the ratio of forcing amplitude to background rotation) is greater than about 0.3. The sidewall boundary layer loses stability to Taylor-Görtler-type instability during the retrograde phase of the libration, and the bulk flow is far from solid-body rotation [28,29]. With other axisymmetric periodic forcings, such

as the axial oscillations of the sidewall, symmetry breaking also does not occur if the corresponding Rossby number is sufficiently small (of order 1 or less) [23]. In the axial direction, the Kelvin modes have either odd or even parity, depending on whether the number of axial half-wavelengths is even or odd. In this study, we investigate the response to periodic forcing that is axisymmetric and is parameterized by a phase in the forcing such that in general it has no axial parity symmetry, but for some values of the phase parameter the forcing has either odd or even axial symmetry.

We select a simple geometry, a circular cylinder, and a class of perturbations that allows us to explore the role of symmetry. In order to keep the flow relatively simple, the chosen perturbations do not alter the direction of the mean rotation vector, keeping it aligned with the cylinder axis. This, together with restricting the forced perturbations to be of small amplitude, keeps the flow axisymmetric. Specifically, we consider the split-cylinder arrangement, where the cylinder is split at midheight and the two halves rotate differentially. Both halves rotate very fast so that their rotation period is very short compared to the viscous diffusion time scale, and the periodic modulations of their mean rotation rates are of very small magnitude. We impose the same period of modulation on the two halves, so that the system is periodically forced, but consider variations in the phases. This phase variation allows us to consider forcings that are either symmetric or nonsymmetric about the cylinder midheight. In particular, when the two cylinder halves are modulated in phase, the modulation is the well-studied libration case [28–33]. In this case, the system is equivariant to a reflection about the midheight. In contrast, when the two halves are modulated exactly out of phase, the system is equivariant to a spatio-temporal symmetry corresponding to the reflection composed with a half-period translation in time, and for any other phase difference there is no spatial or spatio-temporal symmetry in the axial direction. In the following sections, we report on numerical simulations detailing how the various forced modulations lead to different responses in the flow that depend not only on the frequency (as has been previously studied), but also on the phase difference, and how the dependence on the phase difference is intrinsically tied to the symmetry of the system.

II. GOVERNING EQUATIONS AND NUMERICAL METHODS

Consider a circular cylinder of radius a and height h, filled with a fluid of kinematic viscosity ν, rotating with a mean angular speed Ω. The cylinder is split in two at its midheight. The rotations of the two halves are subjected to modulations with the same amplitude and frequency, but with a relative phase difference between the two. The flow is governed by the Navier-Stokes equations, which are nondimensionalized by using a as the length scale and $1/\Omega$ as the time scale to give

$$(\partial_t + \boldsymbol{u}\cdot\boldsymbol{\nabla})\boldsymbol{u} = -\boldsymbol{\nabla} p + \frac{1}{\mathrm{Re}}\nabla^2\boldsymbol{u}, \quad \boldsymbol{\nabla}\cdot\boldsymbol{u} = 0, \tag{1}$$

where $\mathrm{Re} = \Omega a^2/\nu$ is the Reynolds number, p is the pressure, and $\boldsymbol{u} = (u,v,w)$ is the velocity field in cylindrical coordinates $(r,\theta,z) \in [0,1]\times[0,2\pi]\times[-\gamma/2,\gamma/2]$, where $\gamma = h/a$ is the aspect ratio, and the corresponding vorticity field is $\boldsymbol{\nabla}\times\boldsymbol{u} = (\xi,\eta,\zeta)$. In rotating flows, the Ekman number is often used instead of the Reynolds number, where $\mathrm{Ek} = \nu/(2\Omega h^2) = 1/(2\mathrm{Re}\,\gamma^2)$.

The boundary conditions are no-slip; on all walls the radial and axial velocity components are zero, $u = w = 0$, and only the azimuthal component is nontrivial:

$$\begin{aligned}
&\text{top endwall, } z = \gamma/2: && v = r[1+\alpha\sin(\omega t+\phi)],\\
&\text{bottom endwall, } z = -\gamma/2: && v = r[1+\alpha\sin(\omega t)],\\
&\text{top half of sidewall, } r = 1,\ z\in(0,\gamma/2]: && v = 1+\alpha\sin(\omega t+\phi),\\
&\text{bottom half of sidewall, } r = 1,\ z\in[-\gamma/2,0): && v = 1+\alpha\sin(\omega t),
\end{aligned} \tag{2}$$

where α, ω, and ϕ are the amplitude, frequency and phase of the modulation. The forcing amplitude α can be thought of as Rossby number Ro measuring the differential rotation with respect to the background rotation. A schematic of the flow system is shown in Fig. 1.

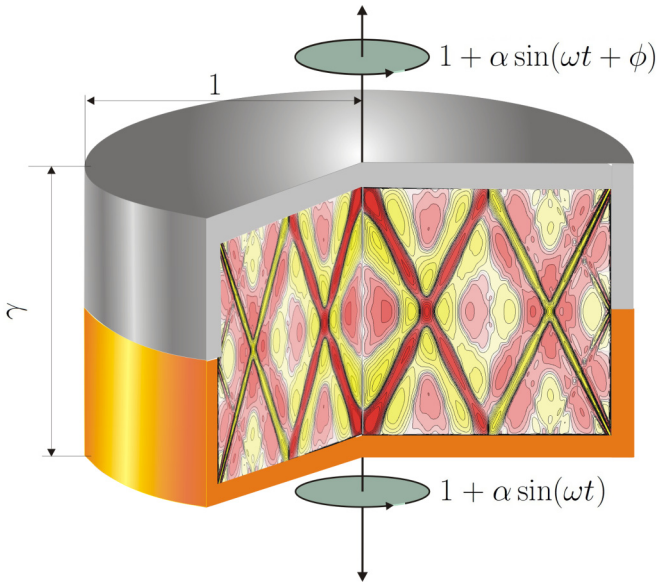

FIG. 1. Schematic of the flow system. The inset shows azimuthal vorticity η for $\mathrm{Re} = 10^6, \gamma = 1, \alpha = 10^{-4}$, $\omega = 0.88$, and $\phi = \pi$.

Since we are interested in the response to small-amplitude periodic perturbations to solid-body rotation, we shall fixed $\alpha = 10^{-4}$. For such weak forcing, the flow is expected to remain axisymmetric [23,28,29], and so we only consider here the axisymmetric Navier-Stokes equations. The axisymmetric Navier-Stokes equations (1) together with the boundary conditions (2) are solved numerically using a second-order time-splitting method, with space discretized using Chebyshev collocation points in r and z:

$$\boldsymbol{u}(r,z,t) = \sum_{n=0}^{2n_r+1} \sum_{m=0}^{n_z} \hat{\boldsymbol{u}}_{mn}(t)\Xi_n(r)\Xi_m(2z/\gamma), \tag{3}$$

where Ξ_n is the nth Chebyshev polynomial. The spectral solver is based on that described in Ref. [34], and it has been used extensively in a wide variety of enclosed cylinder flows. Since the system is harmonically forced, it is convenient to have an integer number of time steps n_t per modulation period $\tau = 2\pi/\omega$, such that the time step is $\delta t = \tau/n_t$. For the cases presented here, the required time resolution was $n_t = 10000$ and the spatial resolution was $n_r = 150$ and $n_z = 151$. This resolution provides at least seven collocation points in the boundary layers ensuring that they are well resolved (see Sec. III A for details regarding the boundary layers).

The discontinuous sidewall boundary condition can lead to Gibb's phenomenon when using a spectral solver. To avoid this, the discontinuity was regularized over a small distance. Specifically, the boundary condition for v at the sidewall is replaced by

$$\begin{aligned} v(r=1,\theta,z) &= 1 + \alpha \tanh(\epsilon z)\sin(\omega t + \phi), \quad && \text{for } z \in (0,\gamma/2], \\ v(r=1,\theta,z) &= 1 + \alpha \tanh(\epsilon z)\sin(\omega t), && \text{for } z \in [-\gamma/2,0), \end{aligned} \tag{4}$$

where ϵ governs the distance over which the discontinuity is smoothed out. Based on studies of this type of regularization for the same cylindrical geometry [35–37], $\epsilon = 50$ was selected. When the phase difference $\phi = 0$ (corresponding to libration), the boundary conditions are not discontinuous and no regularization is used. Note also that no regularization is needed at the corners; the boundary conditions are not discontinuous there.

The axisymmetric Navier-Stokes equations are invariant to arbitrary translations in time and to a reflection in z; the action of these symmetries on the velocity $\boldsymbol{u}$ and the vorticity $\boldsymbol{\nabla}\times\boldsymbol{u}=(\xi,\eta,\zeta)$ are

$$\begin{aligned}\mathcal{T}_\rho(u,v,w,\xi,\eta,\zeta)(r,z,t)&=(u,v,w,\xi,\eta,\zeta,)(r,z,t+\rho),\quad \text{for any real } \rho,\\ \mathcal{K}(u,v,w,\xi,\eta,\zeta)(r,z,t)&=(u,v,-w,-\xi,-\eta,\zeta)(r,-z,t).\end{aligned}\tag{5}$$

However, the boundary conditions (2) are not invariant to either of these symmetries in general. The system (equations and boundary conditions) is equivariant to a specific temporal symmetry $\mathcal{T}_\tau$ due to the harmonic forcing, for any phase difference ϕ. Also, for any value of ϕ, the flow for $-\phi$ is obtained from the flow for ϕ by applying $\mathcal{T}_{-\phi/\omega}\mathcal{K}$ to it, so that only $\phi\in[0,\pi]$ need be considered. The system is invariant to the reflection $\mathcal{K}$ only for $\phi=0$ (libration). For $\phi=\pi$, where the two cylinder halves are half a period out of phase, the system is invariant to the spatio-temporal reflection $\mathcal{T}_{\tau/2}\mathcal{K}=\mathcal{H}$, whose action is

$$\mathcal{H}(u,v,w,\xi,\eta,\zeta)(r,z,t)=(u,v,-w,-\xi,-\eta,\zeta)(r,-z,t+\tau/2).\tag{6}$$

For other values of ϕ, there are no spatial or spatio-temporal symmetries.

The aim of this study is to investigate the response to harmonic forcing in a regime that is close to the linear inviscid regime. This regime is asymptotically reached with $\mathrm{Re}\to\infty$ and $\alpha\to 0$. Numerically, we approximate this regime by taking Re large and α small. Specifically, in this study we fix $\mathrm{Re}=10^6$ and $\alpha=10^{-4}$, and consider variations in the forcing frequency, $\omega\in(0,2]$, and phase, $\phi\in[0,\pi]$. Note that $\mathrm{Re}=10^6$ corresponds to Ekman number $\mathrm{Ek}\sim 5\times10^{-7}$ (depending on γ), which is one to two orders of magnitude smaller than what is typically accessible in laboratory experiments involving measurements of inertial waves and beams.

III. RESULTS

A. Response with $\phi=\pi$

We begin by considering the response when the modulations of the two cylinder halves are out of phase by exactly half a period, i.e., $\phi=\pi$. The consequences of changing the forcing frequency are illustrated in Fig. 2, which shows snapshots of the azimuthal vorticity η in a meridional plane, $(r,z)\in[0,1]\times[-\gamma/2,\gamma/2]$, for several different ω. These and all subsequent contour plots of η in this paper are shown at the same phase of the modulation, corresponding to when $t=(k+1/2)\tau$, with k an arbitrary integer and $\tau=2\pi/\omega$ is the modulation period. Also, all the contour plots of η use the same contour levels and color map (detailed in the caption of Fig. 2), so that they can all be directly compared for the different values of ω, γ, and ϕ used. As ω varies, the beam angle changes in accord with the dispersion relation. The beams emerging from the corners are more intense than those emerging from the sidewall split, irrespective of the value of ω. This is due to the secondary flow in the endwall boundary layers being periodically pumped into the corner region, resulting in a large-amplitude perturbation there, whereas the boundary layer flow in the region of the sidewall split is relatively weak. Furthermore, the finite viscosity and nonlinearity lead to constructive and destructive interactions between the beams as they intersect, producing large variations in the intensity of η with small changes in ω. The online movie [38] shows an animation of η contours, with each frame corresponding to $\omega=0.01i$ for $i\in[2,200]$, illustrating how the beams behave as they cross and reflect off walls and the axis.

In order to quantify the intensity of the response in the bulk to the harmonic forcing, we use the maximum of $|\eta|$ (which is zero for solid-body rotation) over the forcing period τ and the cylindrical domain $\mathcal{D}$, $\eta_\mathrm{f}=\max_{\mathcal{D}}^{\tau}|\eta|$. Figure 3 shows how η_f varies with ω; the figure includes results for $\omega=0.01i$ with $i\in[2,200]$. For $\omega\in(0.5,1.8)$ there is very little variation in η_f, which is in sharp contrast to what one would expect from viewing the η contours in Fig. 2 and the online movie [38], which give the impression of very intense η for particular values of ω. On closer inspection, the lack of peak responses in Fig. 3 is attributable to having used the whole cylindrical domain to determine

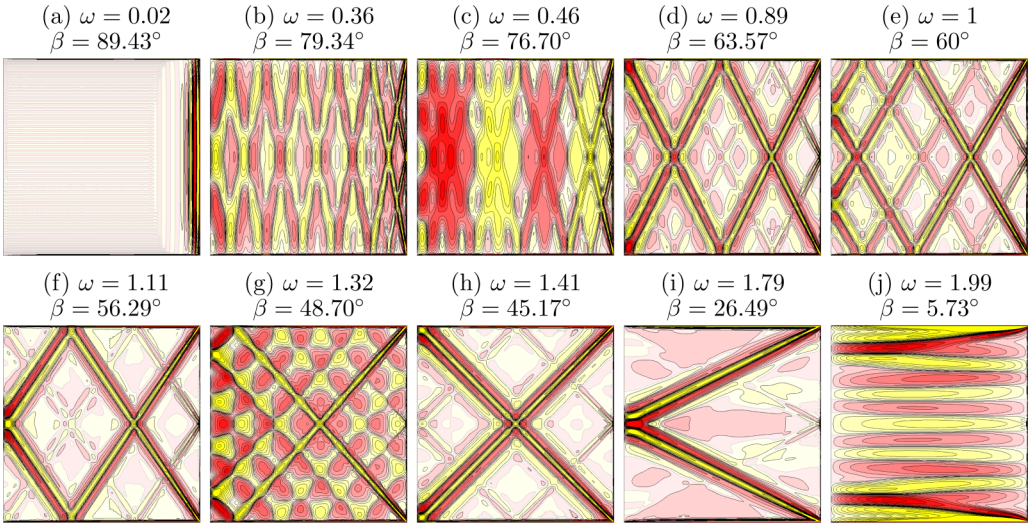

FIG. 2. Azimuthal vorticity contours in the meridional plane $(r,z) \in [0,1] \times [-\gamma/2,\gamma/2]$, with $\phi = \pi$ at various ω as indicated (the corresponding beam angle β according to the dispersion relation is also indicated). An animation is available online [38]. There are 10 contour levels in the range $\eta \in [-0.0005,0.0005]$, quadratically spaced, with positive being red and negative being yellow. Note that all isocontour plots in this paper use the same contour levels and color map.

η_f; the maximum in η occurs in the very thin boundary layers on the top and bottom endwalls. Hence, in order to quantify the response to the modulation in the bulk flow, the contributions from the boundary layers should be excluded [23,28,39].

We now estimate the boundary layer thickness in order to exclude their contribution. The thickness of the endwall boundary layers varies with ω, as is to be expected for an oscillating Ekman boundary layer. This type of boundary layer was previously studied for a librating cylinder [30], and the same analysis is applicable to the split cylinder with arbitrary ϕ. In terms of the nondimensional parameters used here, the boundary layer analysis of Wang [30] gives the endwall boundary layer thickness, for $\omega < 2$, to be $\delta = c/\sqrt{|\omega - 2|\mathrm{Re}}$, where δ is the boundary layer thickness divided by the height of the cylinder and c is a constant of proportionality. In order to compare the boundary layer thickness obtained from our simulations (DNSs) with the estimates of Ref. [30], we have measured the thickness of the boundary layer using the azimuthal vorticity, taking the edge of the boundary layer to be where the fluid is rotating almost as solid body rotation, with $\eta \approx 0$. Although the endwall boundary layer is not of uniform thickness, the variations are negligible, and so we report the thickness at $r = 0.8$. Furthermore, even though the boundary layer is oscillatory, its thickness

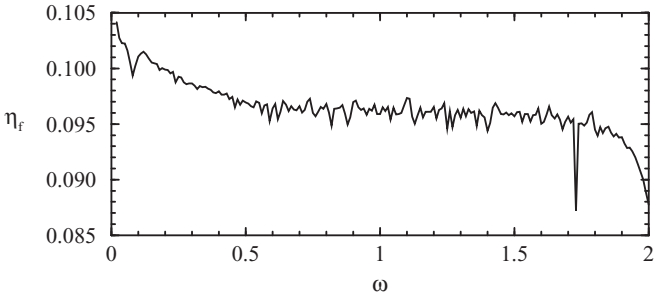

FIG. 3. Variation of η_f with forcing frequency ω for $\gamma = 1$ and $\phi = \pi$.

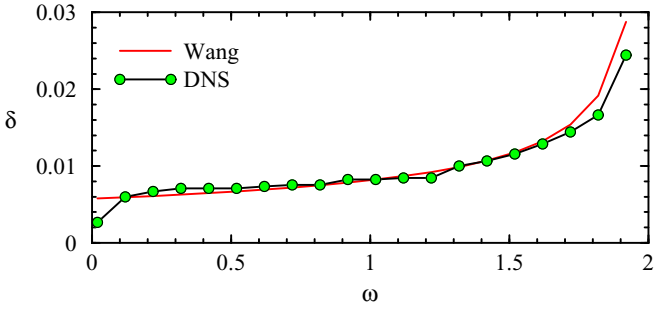

FIG. 4. Endwall boundary layer thickness δ obtained from simulations (DNSs) and estimated using Wang's theory [30] with $c = 8.14$.

is time invariant. This was already noted for the libration case, with $\phi = 0$, [29], and here we have also found this to be the case for $\phi \neq 0$.

Figure 4 shows a comparison between δ obtained from simulations (DNSs) and the theoretical prediction from Wang [30], with $c = 8.14$. The agreement is generally very good, with some discrepancies at the extreme values of ω. For $\omega \approx 2$, Wang's estimate becomes unbounded. Determining δ from the simulations for $\omega \approx 2$ is also troublesome as the beams at these frequencies are nearly horizontal, and it becomes difficult to distinguish between the edge of the boundary layer and the beams.

With an estimate of the boundary layer thickness δ in hand, we now consider the maximum of $|\eta|$ over a period and over the cylindrical domain excluding the boundary layer regions, $\eta_b = \max^{\tau}_{\mathcal{D}/B} |\eta|$. The thickness of the endwall boundary layers is calculated using Wang's scaling, with a modification to avoid the unrealistic effect of δ becoming unbounded for $\omega \sim 2$. The modification is to fix the maximum thickness for the exclusion zone at the endwalls to be no larger than 4% of the cylinder height. In contrast, the sidewall boundary layer thickness does not vary with ω, and a fixed value of 0.66% of the cylinder radius is excluded for all cases. The robustness of the results to variations in the excluded boundary layer regions was checked by using slightly different multiples of δ to define the exclusion zone. Figure 5 shows η_b determined using various multiples near one of δ to define the boundary layer exclusion zones. It is evident that if all of the boundary layer is not removed when computing η_b, much of the response is swamped by boundary layer vorticity contributions. The difference in η_b between using 1.16δ and 0.92δ is very small, whereas η_b is noticeably larger for 0.70δ, especially for $\omega \in (0.5, 1.8)$, this being due to residual contributions from the parts of the boundary layers that were not excluded. Hence all the results we will present for η_b will use 1.16δ to ensure that the boundary layer is entirely excluded. Furthermore, the value of η_b at the peaks is

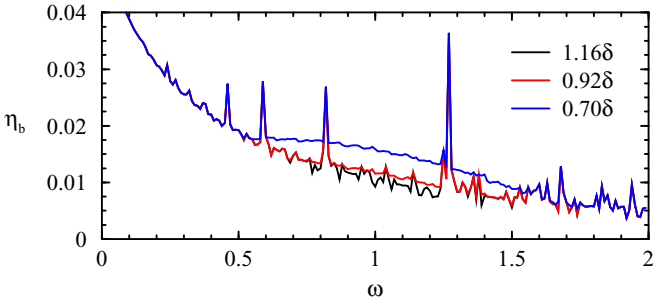

FIG. 5. Variation of η_b with ω, for $\gamma = 1$ and $\phi = \pi$, with the excluded portions of the boundary layers indicated.

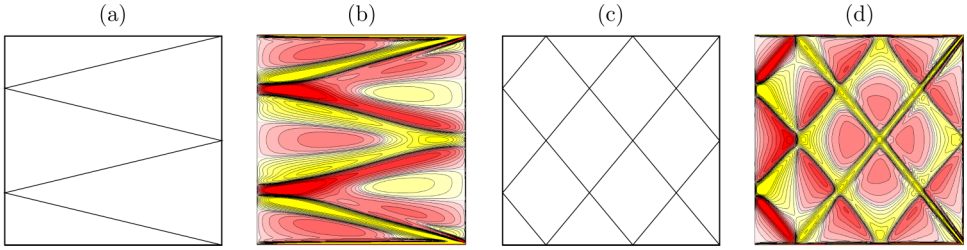

FIG. 6. Retracing rays (a) R_{41} at $\omega = 1.94$, (c) R_{45} at $\omega = 1.25$ and (b, d) η contours at the corresponding frequencies with $\phi = \pi$.

invariant to how much of the boundary layer is excluded, indicating that the peaks are due to a bulk flow response to the modulations. It is also interesting to note that for $\omega \in (0.5, 1.8)$, $\eta_b/\eta_f \sim 0.1$.

B. Nonlinear waves beams, inviscid Kelvin modes, and retracing rays

In order to determine how the bulk flow responds to the modulations, particularly for frequencies corresponding to peak values in η_b, we check to see if those frequencies correspond to either low-order retracing rays or low-order Kelvin modes. The retracing rays are characteristics of the linear inviscid problem that retrace themselves after a certain number of reflections at the walls (and the axis). For the cases in which the beams only emerge from the corners, such as the $\phi = 0$ libration case, the corresponding retracing rays can be described by the number of reflections in the axial direction, $(n-1)$, and in the radial direction, $(k-1)$ [23]. Using n, k, and the aspect ratio of the cylinder, the beam angle is $\beta = \arccos(\omega/2) = \arccos(2n/\sqrt{n^2 + k^2\gamma^2})$. With $\phi = \pi$, since the cylinder is split exactly in half, the retracing rays associated with beams starting at a corner and ending at the split, or starting and ending at the split, are equivalent to the retracing rays associated only with corner sources but for a cylinder of aspect ratio $\gamma/2$. These cases are equivalent to the retracing rays with k an even integer, associated only to corner beams in the cylinder of aspect ratio γ. Therefore, no extra cases have to be considered to account for the split cylinder geometry. Two examples of such retracing rays, R_{41} and R_{45}, are shown in Figs. 6(a) and 6(c), together with the contours of η at the corresponding values of ω for $\phi = \pi$ in Figs. 6(b) and 6(d).

The peaks in η_b could also correspond to resonant forcing at the frequency of a low-order Kelvin mode. Kevin modes are the eigenfunctions of the inviscid Euler equations linearized about solid-body rotation. The azimuthal vorticity of the axisymmetric Kelvin eigenmodes K_{nk} are given by $\eta_{nk}(r,z) = J_1(\sigma_k r)\sin(n\pi[z/\gamma + 1/2])$, where n and k are positive integers and the frequency associated with K_{nk} is $\omega = 2\cos[\arctan(\gamma\sigma_k/n\pi)]$; see Ref. [23] for details.

The frequencies associated with the low-order retracing rays R_{nk} and the low-order Kelvin modes K_{nk}, with $n \leqslant 5$ and $k \leqslant 5$, for three different γ, are listed in Table I. Note that in general, the frequencies associated with R_{nk} and K_{nk} do not coincide. Figure 7 shows the bulk flow response η_b to the modulation for three different aspect ratios; included are red squares corresponding to the frequencies associated with the low-order retracing rays and black triangles corresponding to the low-order Kelvin modes that are listed in Table I. What becomes clear from the figure is that the predominant peaks in $\eta_b(\omega)$ do not correspond to retracing rays, but that they in fact coincide with the frequencies corresponding to K_{1k} with $k \in [1,4]$. This feature of the bulk flow response is independent of γ.

The first row of Fig. 8 shows azimuthal vorticity contours of the Kelvin modes K_{1k} with $k \in [1,4]$, and the subsequent rows show the azimuthal vorticity contours from the simulations at the same frequencies, with different rows corresponding to the three aspect ratios shown in Fig. 7. Although the beams emanating from the corners and the sidewall split are striking, it is also striking that the bulk flow η has the same spatial distribution as in the Kelvin modes (compare red and yellow regions). Also evident from Fig. 8 is that for all the considered γ, the beams are very close to being

TABLE I. Frequencies ω associated with retracing rays R_{nk} and Kelvin modes K_{nk}, for $n \in [1,5]$ and $k \in [1,5]$, and γ as indicated.

	$\gamma = 1$	$\gamma = 0.8$	$\gamma = 0.6$		$\gamma = 1$	$\gamma = 0.8$	$\gamma = 0.6$
R_{11}	1.4142	1.5617	1.7150	K_{11}	1.2681	1.4315	1.6140
R_{12}	0.8944	1.0600	1.2804	K_{12}	0.8174	0.9769	1.1962
R_{13}	0.6325	0.7692	0.9713	K_{13}	0.5901	0.7202	0.9152
R_{14}	0.4851	0.5965	0.7692	K_{14}	0.4590	0.5654	0.7315
R_{15}	0.3922	0.4851	0.6325	K_{15}	0.3747	0.4638	0.6059
R_{21}	1.7889	1.8570	1.9157	K_{21}	1.7075	1.7975	1.8782
R_{22}	1.4142	1.5617	1.7150	K_{22}	1.3343	1.4916	1.6616
R_{23}	1.1094	1.2804	1.4866	K_{23}	1.0509	1.2222	1.4345
R_{24}	0.8944	1.0600	1.2804	K_{24}	0.8531	1.0156	1.2359
R_{25}	0.7428	0.8944	1.1094	K_{25}	0.7128	0.8608	1.0731
R_{31}	1.8974	1.9325	1.9612	K_{31}	1.8527	1.9019	1.9430
R_{32}	1.6641	1.7647	1.8570	K_{32}	1.6043	1.7184	1.8261
R_{33}	1.4142	1.5617	1.7150	K_{33}	1.3592	1.5137	1.6787
R_{34}	1.2000	1.3679	1.5617	K_{34}	1.1550	1.3248	1.5252
R_{35}	1.0290	1.2000	1.4142	K_{35}	0.9933	1.1635	1.3803
R_{41}	1.9403	1.9612	1.9779	K_{41}	1.9130	1.9430	1.9673
R_{42}	1.7889	1.8570	1.9157	K_{42}	1.7463	1.8261	1.8964
R_{43}	1.6000	1.7150	1.8238	K_{43}	1.5544	1.6787	1.7990
R_{44}	1.4142	1.5617	1.7150	K_{44}	1.3723	1.5252	1.6875
R_{45}	1.2494	1.4142	1.6000	K_{45}	1.2131	1.3803	1.5721
R_{51}	1.9612	1.9749	1.9858	K_{51}	1.9430	1.9630	1.9789
R_{52}	1.8570	1.9048	1.9448	K_{52}	1.8261	1.8834	1.9318
R_{53}	1.7150	1.8030	1.8818	K_{53}	1.6787	1.7758	1.8642
R_{54}	1.5617	1.6845	1.8030	K_{54}	1.5252	1.6550	1.7824
R_{55}	1.4142	1.5617	1.7150	K_{55}	1.3803	1.5323	1.6928

retracing; this is a consequence of the frequency associated with K_{11} being close to the frequency associated with R_{45} (they differ by about 1%–2%; however, this is not necessarily a small difference). The beams for the other frequencies in the figure are also close to higher-order retracing rays (the corresponding frequencies are not listed in the Table I). The point, however, is not that there are retracing rays arbitrary close to the simulated peaks, but rather that the low-order retracing rays do not result in peaks. Notice also that for $\phi = \pi$ the flow is $\mathcal{H}$-symmetric, and so are the odd axial Kelvin modes, which are associated with the bigger peaks in Fig. 7.

C. Influence of the phase difference

We now consider the impact of the phase difference between the harmonic forcing of the two cylinder halves. Figure 9 shows the variation of η_b with ω for five different values of ϕ. For $\phi = \pi$ [Fig. 9(a), which essentially is the same as Fig. 6(a) and included here for ease of comparison with the rest of the cases], the peaks in η_b occur at frequencies ω corresponding to the frequencies of the leading odd axial Kelvin modes, K_{1j} with $j \in [1,4]$, as discussed in the previous section. For $\phi = 3\pi/4$ [Fig. 9(b)], the larger peaks still correspond to the same Kelvin modes. Further decreasing ϕ [Figs. 9(c) and 9(d)], these same peaks are still present, but their intensity is lower and some other peaks are evident. Finally, for $\phi = 0$ [the libration case, Fig. 9(e)], the peaks corresponding to the odd axial Kelvin modes disappear, and instead, the peaks that are present correspond to frequencies of even axial Kelvin modes, K_{2j} with $j \in [1,3]$; some of these are the additional peaks that were found in Figs. 9(c) and 9(d) and are absent in Fig. 9(a).

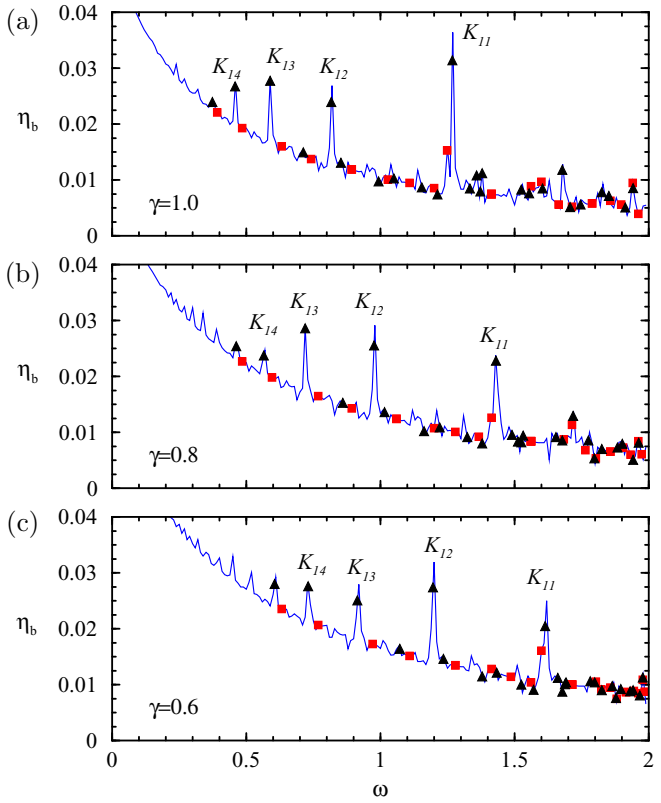

FIG. 7. Variation with forcing frequency of the maximum value of azimuthal vorticity over the forcing period in the bulk flow (excluding the endwall and sidewall boundary layers to the level 1.16δ) for $\phi = \pi$ and γ as indicated. The red squares are the responses at frequencies corresponding to low-order retracing rays and the black triangle are the responses at frequencies corresponding to low-order Kelvin mode frequencies.

Figure 10 shows snapshots of η at the frequencies corresponding to the odd Kelvin modes, which correspond to the frequencies of the stronger peaks in η_b for $\phi = \pi$. The odd Kelvin modes are shown in the first row of the figure, and the other rows correspond to simulations at different ϕ. The flow structure is akin to the superposition of odd axial Kelvin modes and wave beams. With decreasing ϕ, the flow is slightly different, it loses the features associated with the odd axial Kelvin mode, but the beam structure persists. When $\phi = 0$, the flow no longer has features related to an odd axial Kelvin mode, but instead it is similar to an even axial Kelvin mode. This behavior with variable ϕ is consistent with the flow for $\phi = 0$ being $\mathcal{H}$ invariant, as are the odd Kelvin modes, whereas for $\phi = \pi$ the flow is $\mathcal{K}$ invariant, as are the even Kelvin modes. These results are congruent with the stronger peaks found for each case in Fig. 9.

In Fig. 11 we consider the leading even axial Kelvin modes in the first row, and the other rows show simulations at the corresponding frequencies for different ϕ. The similarities between the simulations for $\phi = 0$ and the even Kelvin modes is quite striking. With increasing ϕ, the flow still has features in common with the corresponding even Kelvin mode until $\phi = \pi$, in which case the flow characteristics are more similar to an odd Kelvin mode. The results illustrated in Figs. 10 and 11 indicate that the phase difference ϕ is crucial in the selection of which Kelvin mode is resonantly excited, and this selection is predicated by the symmetry of the system.

The influence of ϕ on the behavior of the bulk of the flow is remarkable even for ω not associated with peaks in $\eta_b(\omega)$. Figure 12 shows snapshots of η for $\phi = \pi, 3\pi/4, \pi/2, \pi/4$, and 0 for various ω.

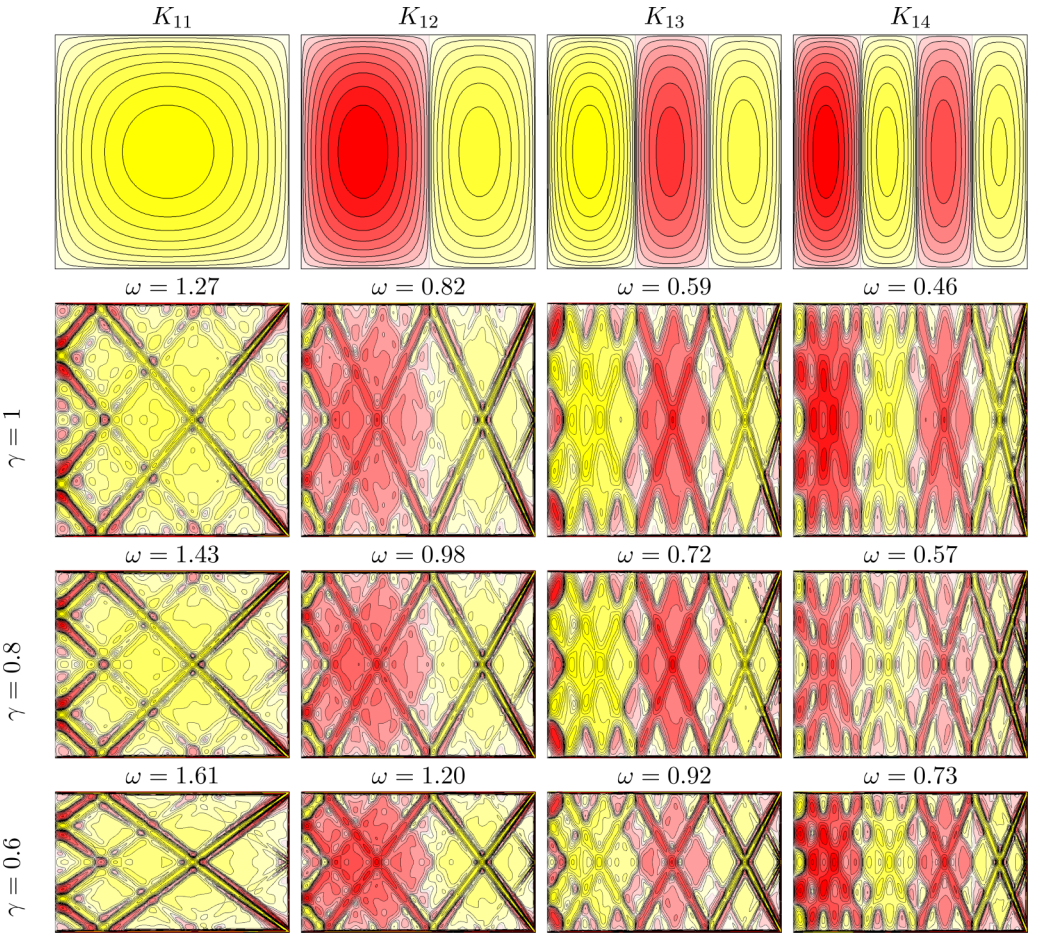

FIG. 8. Comparison between the Kelvin eigenmodes (first row) and azimuthal vorticity contours at the resonant frequency, for $\phi = \pi$ and γ as indicated.

The $\phi = \pi$ states are similar to even Kelvin modes and the $\phi = 0$ states are similar to odd Kelvin modes (similar in the sense that they have the same symmetry, $\mathcal{K}$ or $\mathcal{H}$). However, for the other ϕ values, for which the system is neither $\mathcal{K}$ or $\mathcal{H}$ symmetric, the flows (which are not symmetric) can have similarities with one or the other case, or with neither of the odd or even Kelvin modes.

IV. DISCUSSION AND CONCLUSION

We have studied the response to small-amplitude harmonic forcing in a simple rapidly rotating system whose configuration can be tuned continuously between having a spatial reflection symmetry ($\mathcal{K}$) and a spatio-temporal reflection symmetry ($\mathcal{H}$). The rapid rotation regime corresponds to Ekman numbers $\mathrm{Ek} \sim 10^{-6}$, which is typically the lower limit achieved in laboratory experiments, and the considered forcing amplitude corresponds to a differential rotation Rossby number $\mathrm{Ro} \sim 10^{-4}$. The low Ek puts us in the low-viscosity regime, while $\mathrm{Ro}/\sqrt{\mathrm{Ek}} \ll 1$ is needed for negligible nonlinear effects. We have $\mathrm{Ro}/\sqrt{\mathrm{Ek}} \sim 0.1$, so while the forcing amplitude is small, the response may still be too large to simply neglect nonlinear effects. Nevertheless, typical laboratory experiments have larger $\mathrm{Ro}/\sqrt{\mathrm{Ek}}$ due to signal-to-noise ratio constraints of their measurement techniques. We find that when the forcing has either $\mathcal{K}$ or $\mathcal{H}$ symmetry, the flow responds with peaks at frequencies

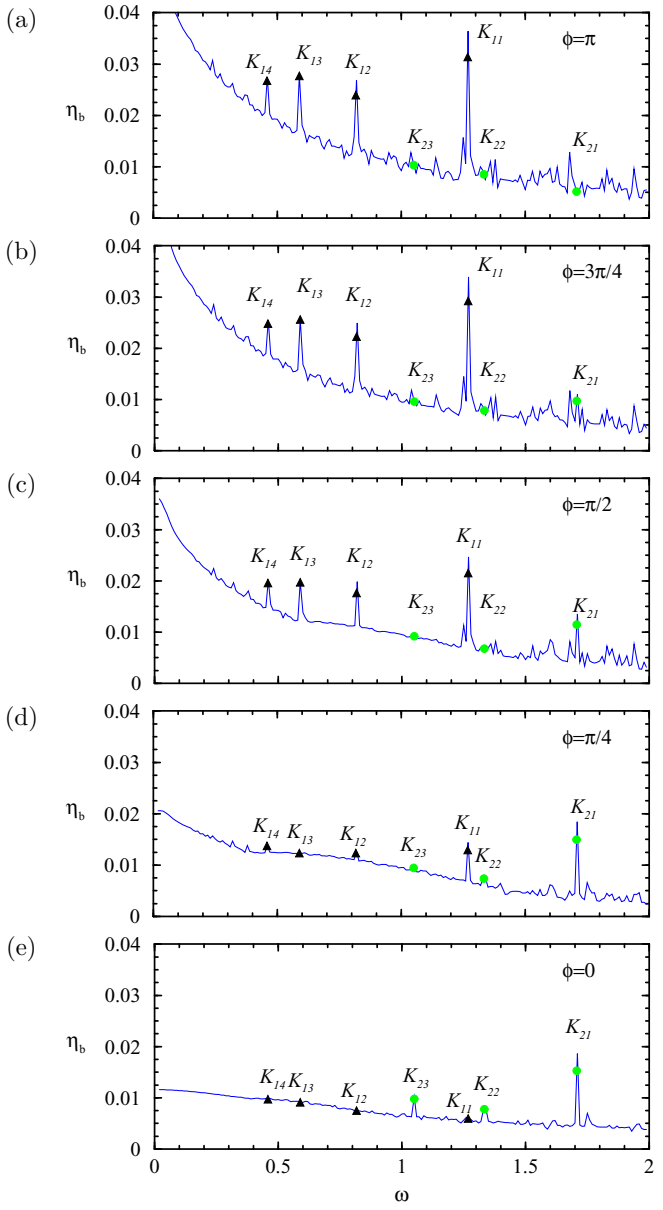

FIG. 9. Variation of η_b with ω, for $\gamma = 1$ and ϕ as indicated. The black triangles are the responses at frequencies corresponding to K_{1k} with $k \in [1,4]$ and the green circles corresponding to K_{2k} with $k \in [1,3]$.

corresponding to low-order Kelvin modes with the same symmetry. This is consistent with the experimental observation of Ref. [25], but their system, a librating cube, had but a single symmetry group ($\mathcal{K}$). They concluded that it is of interest to consider other forcings that result in a system with what they call antisymmetric modes (essentially this would correspond to a system with $\mathcal{H}$ symmetry, such as the $\phi = \pi$ case in our problem) to see if the odd axial Kelvin modes would be excited, and indeed we find that they are. They also suggested that it is of interest to examine what happens in systems with broken symmetry, and that corresponds to the cases with $\phi \neq 0$ and $\phi \neq \pi$.

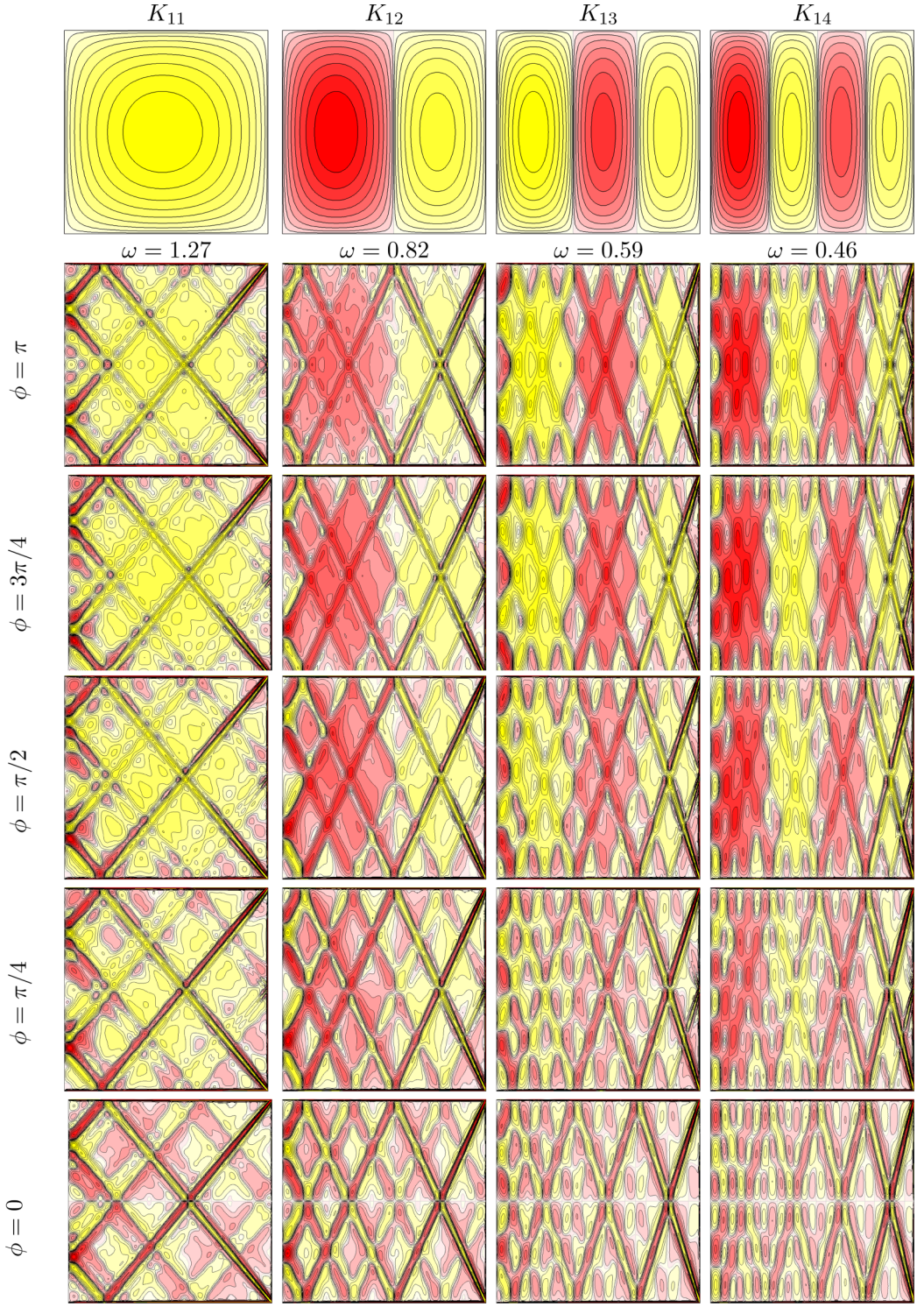

FIG. 10. Comparison between the Kelvin modes and azimuthal vorticity contours at the given frequencies ω, corresponding to peaks in η_b, for $\gamma = 1$ and ϕ as indicated.

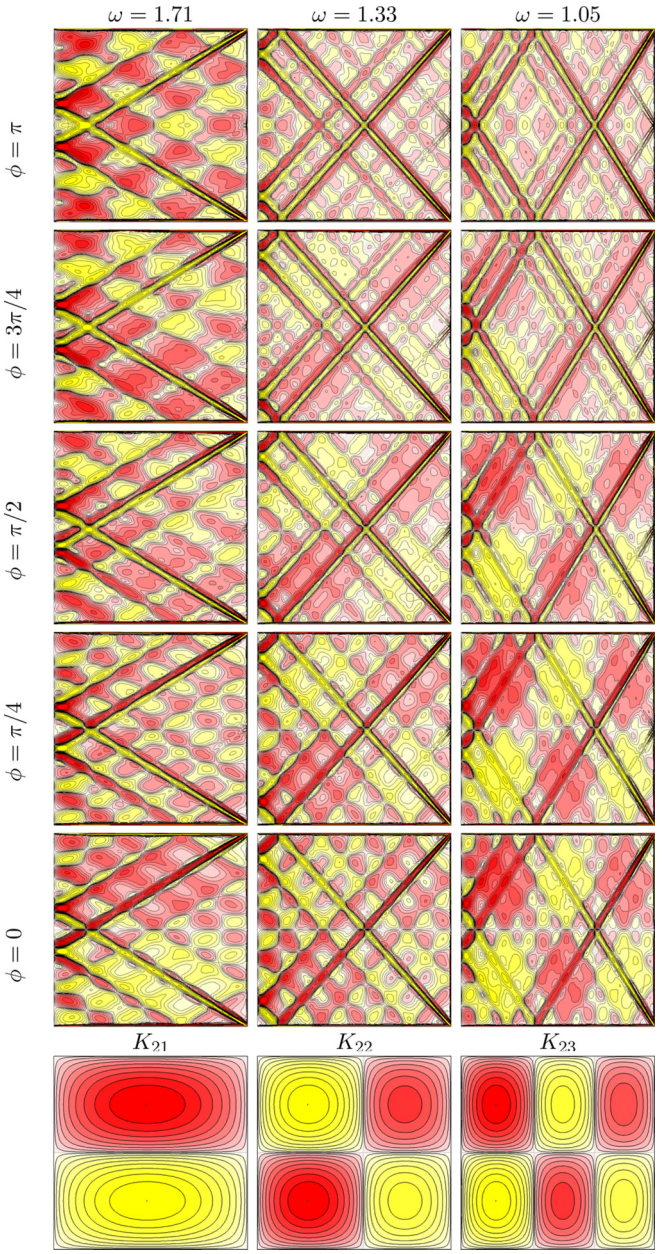

FIG. 11. Comparison between the Kelvin modes and azimuthal vorticity contours at the given frequencies ω, corresponding to peaks in η_b, for $\gamma = 1$ and ϕ as indicated.

We find in these cases that both odd and even Kelvin modes can be excited, and the degree to which one or other is excited depends on the degree to which the symmetries are broken.

Weak perturbations to rapidly rotating flows have responses which are not straight forward to predict. The very rapid rotation limit suggests that viscous effects may be small enough to neglect, and if the imposed perturbation levels are sufficiently small, then nonlinearities may also be negligible. In the classical approach to the problem, viscous terms in the governing equations are neglected,

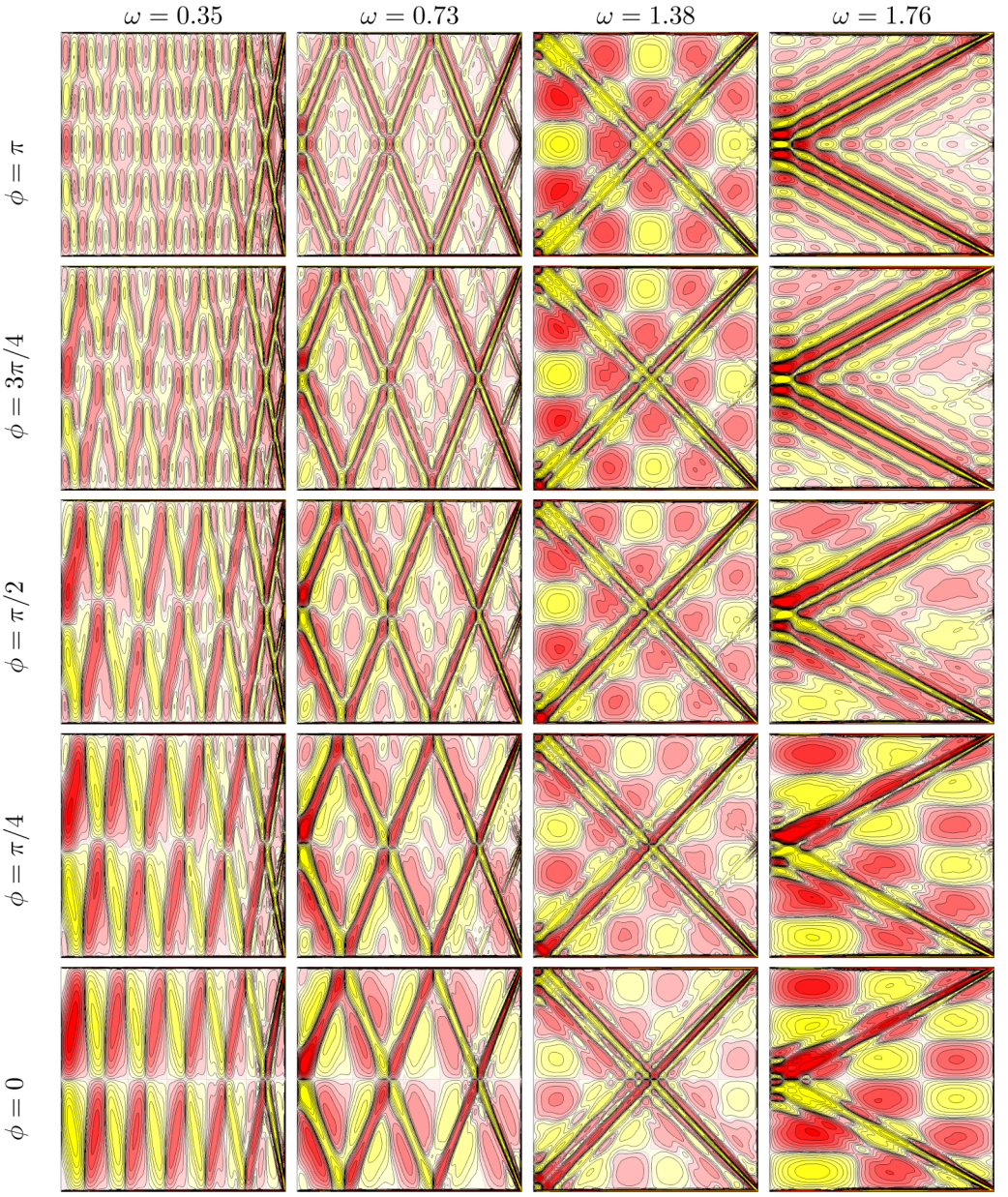

FIG. 12. Azimuthal vorticity contours for $\gamma = 1$ at ω and ϕ as indicated.

and the system is linearized by considering infinitesimal perturbations to solid-body rotation. For perturbation frequencies less than twice the rotation frequency, the resulting linear equation is of hyperbolic form. This oscillator system results from the restoring nature of the Coriolis force. The eigenmodes, Kelvin modes, are neutral, i.e., the real parts of the eigenvalues are zero. However, solid-body rotation is stable (viscous eigenmodes are damped), and the higher order eigenmodes are more rapidly damped. So to observe the eigenmodes in a physical setting, the perturbations need to be continuously applied. The details of this forcing will impact what is observed. For a damped oscillator system, the response is composed of both the eigenmodes of the unforced system

(which are damped and take care of the initial condition) and the forced response which is all that survives after some time. The expectation is that if the harmonic forcing has the spatio-temporal structure of one of the eigenmodes of the unforced system, then it can be resonantly excited with a very small-amplitude forcing. Of course, in practice, one does not have complete control of the spatio-temporal structure of the forcing, but typically only controls boundary forcing at a selected frequency. Nevertheless, in practice, responses that have much in common with the target eigenmode result.

A complication, however, is that the harmonic forcing in the physical system often leads to the formation of boundary layers. In the singularly perturbed problem (neglecting viscous effects) these do not exist. In rapidly rotating flows, a fundamental issue is whether there is a one-to-one correspondence between solutions of the singularly perturbed problem ($\mathrm{Ek} = 0$) and the full problem ($0 < \mathrm{Ek} \ll 1$) [8]. Various asymptotic analyses have tried to address this issue, typically employing expansions based on $\mathrm{Ek}^{1/2}$, but have not been able to show one-to-one correspondence [40]. Then there is the further issue of whether the nonlinear terms are negligible [41]. The problem here is subtle. On the one hand, one relies on resonance in the very low viscosity limit using a very low amplitude forcing to excite an eigenmode to an observable level, but if it is observable it is because the flow deviation away from solid-body rotation is not small, and so nonlinear effects may not be negligible. This issue is addressed in Zhang *et al.* [14] by an asymptotic analysis based on the velocity-pressure formulation that allows the no-slip boundary condition to be explicitly enforced. Their asymptotic results suggest that libration in the small Ek and small Ro limits does not result in any resonances with the linear inviscid modes of axisymmetric containers (they specifically studied the sphere and suggested that their results also applied to the cylinder). In contrast, our simulations with finite but small Ek and Ro do show resonances with low-order Kelvin modes. As indicated above, this may be due to non-negligable nonlinear effects as our $\mathrm{Ro}/\sqrt{\mathrm{Ek}} \sim 0.1$ may not be small enough to be in the asymptotic regime.

The harmonic forcing may excite a low-order eigenmode, but temporally periodic viscous boundary layers are also formed. These tend to drive wave beams into the interior from corners along the characteristics of the linear inviscid system. These beams are omnipresent and become narrower and more intense for smaller Ek. Note that they do not exist in the singularly perturbed system. So now we have that the solutions for $\mathrm{Ek} = 0$ and $0 < \mathrm{Ek} \ll 1$ differ not only in the boundary layer regions, but also throughout the entire flow because of the presence of the beams.

At the end of the day, the details of how a rapidly rotating flow responds to small-amplitude harmonic forcing requires the consideration of the full system of governing equations.

ACKNOWLEDGMENT

This work was supported by U.S. NSF Grant No. CBET-1336410.

[1] W. E. Scott, The large amplitude motion of a liquid-filled gyroscope and the non-interaction of inertial and Rossby waves, J. Fluid Mech. **72**, 649 (1975).
[2] R. Manasseh, Visualization of the flow in precessing tanks with internal baffles, AIAA J. **31**, 312 (1993).
[3] W. V. R. Malkus, Precession of the Earth as the cause of geomagnetism, Science **160**, 259 (1968).
[4] A. Tilgner, Precession driven dynamos, Phys. Fluids **17**, 034104 (2005).
[5] D. H. Kelley, S. A. Triana, D. S. Zimmerman, A. Tilgner, and D. P. Lathrop, Inertial waves driven by differential rotation in a planetary geometry, Geophys. Astrophys. Fluid Dyn. **101**, 469 (2007).
[6] M. Le Bars, D. Cebron, and P. Le Gal, Flows driven by libration, precession, and tides, Annu. Rev. Fluid Mech. **47**, 163 (2015).
[7] Lord Kelvin, Vibrations of a columnar vortex, Phil. Mag. **10**, 155 (1880).

[8] H. P. Greenspan, *The Theory of Rotating Fluids* (Cambridge University Press, Cambridge, 1968).
[9] P. A. Davidson, *Turbulence in Rotating, Stratified and Electrically Conducting Fluids* (Cambridge University Press, Cambridge, 2013).
[10] K. D. Albridge and A. Toomre, Axisymmetric inertial oscillations of a fluid in a rotating spherical container, J. Fluid Mech. **37**, 307 (1969).
[11] R. F. Gans, On the precession of a resonant cylinder, J. Fluid Mech. **41**, 865 (1970).
[12] R. Manasseh, Breakdown regimes of inertia waves in a precessing cylinder, J. Fluid Mech. **243**, 261 (1992).
[13] P. Meunier, C. Eloy, R. Lagrange, and F. Nadal, A rotating fluid cylinder subject to weak precession, J. Fluid Mech. **599**, 405 (2008).
[14] K. Zhang, K. H. Chan, X. Liao, and J. M. Aurnou, The non-resonant response of fluid in a rapidly rotating sphere undergoing longitudinal libration, J. Fluid Mech. **720**, 212 (2013).
[15] G. Backus and M. Rieutord, Completeness of inertial modes of an incompressible inviscid fluid in a corotating ellipsoid, Phys. Rev. E **95**, 053116 (2017).
[16] Y. Duguet, Simulation numérique de l'instabilité dans un cylindre de daz tournant soumis à une compression périodique, Ph.D. thesis, L'école Centrale de Lyon, 2004.
[17] T. Albrecht, H. M. Blackburn, J. M. Lopez, R. Manasseh, and P. Meunier, Triadic resonances in precessing rapidly rotating cylinder flows, J. Fluid Mech. **778**, R1 (2015).
[18] F. Marques and Juan M. Lopez, Precession of a rapidly rotating cylinder flow: Traverse through resonance, J. Fluid Mech. **782**, 63 (2015).
[19] W. W. Wood, Properties of inviscid, recirculating flows, J. Fluid Mech. **22**, 337 (1965).
[20] W. W. Wood, An oscillatory disturbance of rigidly rotating fluid, Proc. Roy. Soc. Lond. A **293**, 181 (1966).
[21] A. D. McEwan, Inertial oscillations in a rotating fluid cylinder, J. Fluid Mech. **40**, 603 (1970).
[22] Y. Duguet, J. F. Scott, and L. Le Penven, Oscillatory jets and instabilities in a rotating cylinder, Phys. Fluids **18**, 104104 (2006).
[23] J. M. Lopez and F. Marques, Rapidly rotating cylinder flow with an oscillating sidewall, Phys. Rev. E **89**, 013013 (2014).
[24] I. D. Borcia, V. A. Ghasemi, and U. Harlander, Inertial wave mode excitation in a rotating annulus with partially librating boundaries, Fluid Dynam. Res. **46**, 041423 (2014).
[25] J. Boisson, C. Lamriben, L. R. M. Maas, P. P. Cortet, and F. Moisy, Inertial waves and modes excited by the libration of a rotating cube, Phys. Fluids **24**, 076602 (2012).
[26] P. G. Baines, Forced oscillations of an enclosed rotating fluid, J. Fluid Mech. **30**, 533 (1967).
[27] H. P. Greenspan, On the general theory of contained rotating fluid motions, J. Fluid Mech. **22**, 449 (1965).
[28] A. Sauret, D. Cébron, M. Le Bars, and S. Le Dizés, Fluid flows in a librating cylinder, Phys. Fluids **24**, 026603 (2012).
[29] J. M. Lopez and F. Marques, Instabilities and inertial waves generated in a librating cylinder, J. Fluid Mech. **687**, 171 (2011).
[30] C. Wang, Cylindrical tank of fluid oscillating about a state of steady rotation, J. Fluid Mech. **41**, 581 (1970).
[31] A. Rubio, J. M. Lopez, and F. Marques, Interacting oscillatory boundary layers and wall modes in modulated rotating convection, J. Fluid Mech. **625**, 75 (2009).
[32] J. Noir, M. A. Calkins, J. Cantwell, and J. M. Aurnou, Experimental study of libration-driven zonal flows in a straight cylinder, Phys. Earth Planetary Int. **182**, 98 (2010).
[33] F. H. Busse, Zonal flow induced by longitudinal librations of a rotating cylindrical cavity, Physica D **240**, 208 (2011).
[34] I. Mercader, O. Batiste, and A. Alonso, An efficient spectral code for incompressible flows in cylindrical geometries, Comput. Fluids **39**, 215 (2010).
[35] P. Gutierrez-Castillo and J. M. Lopez, Instabilities of the sidewall boundary layer in a rapidly rotating split cylinder, Eur. J. Mech. B–Fluids **52**, 76 (2015).
[36] J. M. Lopez and P. Gutierrez-Castillo, Three-dimensional instabilities and inertial waves in a rapidly rotating split-cylinder flow, J. Fluid Mech. **800**, 666 (2016).

[37] P. Gutierrez-Castillo and J. M. Lopez, Nonlinear mode interactions in a counter-rotating split-cylinder flow, J. Fluid Mech. **816**, 719 (2017).

[38] See Supplemental Material at http://link.aps.org/supplemental/10.1103/PhysRevFluids.2.084802 for an animation of snapshots at the same phase of the period for frequencies $\omega = 0.01i$ for $i \in [2,200]$.

[39] M. Klein, T. Seelig, M. V. Kurgansky, V. A. Ghasemi, I. D. Borcia, A. Will, E. Schaller, C. Egbers, and U. Harlander, Inertial wave excitation and focusing in a liquid bounded by a frustum and a cylinder, J. Fluid Mech. **751**, 255 (2014).

[40] X. Liao and K. Zhang, On viscous decay factors for spherical inertial modes in rotating planetary fluid cores: Comparison between asymptotic and numerical analysis, Phys. Earth Planetary Int. **169**, 211 (2008).

[41] K. Zhang and X. Liao, On the initial-value problem in a rotating circular cylinder, J. Fluid Mech. **610**, 425 (2008).